Journal of
Synchrotron Radiation

ISSN 0909-0495

Received 7 June 2004
Accepted 12 October 2004

In situ synchrotron X-ray studies of ferroelectric thin films

D. D. Fong,[a] J. A. Eastman,[a] G. B. Stephenson,[a] P. H. Fuoss,[a] S. K. Streiffer,[a] Carol Thompson[b] and O. Auciello[a]*

Argonne National Laboratory, 9700 South Cass Avenue, Argonne, IL 60439, USA, and [b]Northern Illinois University, DeKalb, IL 60115, USA. E-mail: auciello@anl.gov

In situ synchrotron X-ray scattering was used to observe both the growth of $PbTiO_3$ films by metal-organic chemical vapour deposition and the behaviour of the ferroelectric phase transition as a function of film thickness. The dependences of growth mode and deposition rate on gas flows and substrate temperature were determined by homoepitaxial growth studies on thick films (>50 nm). These studies facilitated the growth of thin coherently strained $PbTiO_3$ films on $SrTiO_3$ (001) substrates, with thicknesses ranging from 2 to 42 nm. Experiments on the ferroelectric phase transition as a function of film thickness were carried out in these films under controlled mechanical and electrical boundary conditions.

Keywords: thin films; $PbTiO_3$; chemical vapour deposition; ferroelectric phase transition; 180° stripe domains.

1. Introduction

With the integration of ferroelectric materials into microelectronic devices, there has been increased interest in both the growth of ferroelectric thin films and their material properties. $Pb(Zr_xTi_{1-x})O_3$, a commonly used ferroelectric material, can be found in a variety of thin-film applications including nonvolatile memories (Auciello *et al.*, 1998) and microelectromechanical systems (Polla & Francis, 1996; Muralt, 2000). Metal-organic chemical vapour deposition (MOCVD) is a preferred synthesis technique for $Pb(Zr_xTi_{1-x})O_3$, allowing high-density integration onto nonplanar structures with controlled stoichiometry. Improving the crystal quality and ferroelectric properties of these films requires a better understanding of the chemistry and dynamics taking place at the film surface during growth. However, the atomic-scale mechanisms controlling deposition have not been well characterized because few surface-analysis techniques are compatible with the MOCVD vapour-phase environment.

Another area of interest is the effect of the electrical and mechanical boundary conditions on ferroelectric behaviour. Although this has been discussed widely in the theoretical literature (Pertsev *et al.*, 1998; Pertsev & Koukhar, 2000; Bratkovsky & Levanyuk, 2000*a*), there have been few experimental results. For instance, the competition between strain, electric field and polarization in ferroelectric crystals can result in the development of periodic domain patterns (Speck & Pompe, 1994). In particular, 180° stripe domains, which consist of lamellae with alternating signs of polarity, have been observed to form in bulk crystals in order to minimize the energy of the depolarizing field. Theorists have predicted that the formation of such a domain structure in thin films would have significant implications for ferroelectric device performance (Wang *et al.*, 1995; Bratkovsky & Levanyuk, 2000*a*,*b*, 2001). However, until the present work there had been no experimental observation of 180° stripe domains in thin films.

We have addressed several of these issues using a unique apparatus specially designed for *in situ* grazing-incidence X-ray scattering measurements both during and subsequent to film growth. X-ray scattering is the most direct atomic-scale structural probe compatible with the near-atmospheric-pressure reactive environment of MOCVD. By monitoring the crystal truncation rods (CTRs) during growth, we can determine the growth mode and rate as a function of the gas flows and substrate temperature; by watching how the CTRs evolve as a function of temperature, we can study the behaviour of the ferroelectric phase transition for films of varying thicknesses. In this paper, we summarize our recent results on the growth of the prototypical ferroelectric $PbTiO_3$ by MOCVD (Murty *et al.*, 2002) and the observation of 180° stripe domains in these films (Streiffer *et al.*, 2002). We also present new results comparing the growth behaviour using different titanium precursors.

2. Experiment

Grazing-incidence X-ray scattering measurements were conducted at undulator beamline 12-ID-D at the Advanced Photon Source. We performed *in situ* growth of $PbTiO_3$ films in a vertical-flow MOCVD chamber mounted on a horizontal diffraction plane z-axis diffractometer (Stephenson *et al.*,

1999). The fused-quartz walls of the chamber allow studies to be carried out up to 1473 K in oxidizing environments. Penetrating the 2 mm-thick quartz walls requires the use of moderately high-energy X-rays (24 keV). For both growth studies and structural studies of films only a few unit cells thick, the incidence angle is set at the critical angle of $PbTiO_3$ (0.13°), while the incidence angle is fixed at 1° for structural studies of thicker films.

The $PbTiO_3$ films were grown using O_2, tetraethyl lead (TEL) and either titanium isopropoxide (TIP) or titanium tertbutoxide (TTB). Nitrogen was the carrier gas. Films were deposited at 923–1023 K at a total chamber pressure of 10 torr (P_{O_2} = 2.5 torr) on $SrTiO_3$ (001) substrates. More details on the growth conditions can be found by Murty *et al.* (2002). Coherently strained films were used for studies of the ferroelectric phase transition. Relaxed thicker films were used for homoepitaxial growth studies. The single-crystal films replicated the crystal quality of the substrate (mosaic width typically 0.05°).

The ability to perform X-ray scattering experiments in the growth chamber not only allows us to carry out real-time studies of crystal growth, but also to investigate the ferroelectric phase transition at high temperature immediately after growth, avoiding any irreversible relaxation that can occur upon cooling. Furthermore, the growth system can be used to control the PbO vapour pressure over the film and therefore maintain film stoichiometry as well as the equilibrium surface structure (Munkholm *et al.*, 2002).

3. Crystal growth dynamics

3.1. Homoepitaxial growth

Prior to investigations of the ferroelectric phase transition, we performed extensive studies on the homoepitaxial growth of $PbTiO_3$. Growth mechanisms and morphology depend on the gas composition, flow rate, pressure and substrate temperature. The competition between deposition rate, surface mobility and step propagation on the surface determines the preferred growth mode. We consider three homoepitaxial growth modes: step-flow, layer-by-layer and 3D (Stephenson *et al.*, 1999). In the step-flow mode, atoms arriving on the surface attach to existing steps. Since the surface morphology is in a steady state, the CTR intensity remains constant. In the layer-by-layer growth mode, islands nucleate on the terraces between steps and coalesce, and the CTR intensity oscillates in time with each additional layer of growth owing to the cyclic changes in the occupations of neighbouring layers. Finally, in the 3D growth mode, deposited atoms typically remain where they arrive; consequently, the surface roughens rapidly and the CTR intensity decays monotonically. X-ray CTR oscillations are similar to oscillations in surface-sensitive electron diffraction (*e.g.* RHEED), which have been reported for perovskite growth at low pressure by both pulsed laser deposition and molecular beam epitaxy (Rijnders *et al.*, 1997; Terashima *et al.*, 1990; Lippmaa *et al.*, 2000).

Growth was initiated in our MOCVD chamber by injecting either TIP or TTB into the cation precursor flow, with the TEL flow already established. Precautions were taken to stay within the $PbTiO_3$ single-phase field in which excess PbO volatilizes. Growth stops when the TIP or TTB injection is terminated. After growth, we typically observe that the CTR intensity increases back to its original value, indicating that the surface gradually recovers its initial smoothness.

Fig. 1(*a*) shows the time evolution of the 20*L* CTR intensity at L = 0.5 during deposition at various temperatures, with fixed TIP and TEL flows. The strong intensity oscillations show that layer-by-layer growth occurs at all temperatures. At higher temperatures the amplitude of the oscillations diminishes, indicating a gradual tendency toward step-flow growth, consistent with an expected increase in surface mobility. The rapid decay in the oscillations at lower temperatures demonstrates a tendency towards 3D growth. By comparing the growth rates obtained from the period of these oscillations with those obtained by optical methods, we verified that the layer-by-layer oscillation period corresponds to the growth of single-unit-cell layers (Stephenson *et al.*, 1999). As shown in the inset of Fig. 1(*a*), the growth rate, G, is almost independent of temperature for growth with TIP. In contrast, Fig. 1(*b*) shows that for films grown with the TTB precursor the growth rate decreases for substrate temperatures below 973 K at fixed TEL and TTB flows.

For films grown with either TIP or TTB, the growth rate was found to depend linearly on Ti precursor flow within experimental uncertainty; for TTB, this was true for all investigated temperatures. In the case of TIP, the growth mode changed from layer-by-layer to step-flow as G decreased at constant temperature. This was the first experimental demonstration of step-flow growth for MOCVD of a perovskite (Murty *et al.*, 2002).

Fig. 2(*a*) shows the CTR intensity during deposition at various TEL flow rates, with the TIP flows set at 0.26 μmol min^{-1}. The inset shows that G is independent of TEL flow for the TIP precursor. However, the growth mode varies with the TEL flow rate, tending towards step flow as the TEL flow is reduced. This indicates either that the surface mobility increases or that island nucleation or step attachment kinetics change with lower TEL flow. Additional information can be obtained by monitoring the behaviour of the CTR after halting growth. Following deposition, reducing the TEL flow facilitated recovery of a smooth surface. This is consistent with a higher surface mobility at lower TEL flows. Fig. 2(*b*) shows significantly different behaviour for growth with the TTB precursor. In this case, the growth rate increases somewhat with increased TEL flow (inset). After growth, we also observed that reduction of the TEL flow increased the rate of recovery of a smooth surface.

The dependence of the growth process on P_{O_2} was also measured by varying the O_2 fraction in the anion and window purge flows. No changes in the CTR oscillations were observed for O_2 fractions in the range 0.125–1.00, suggesting that neither growth mode nor G is affected by P_{O_2} under our typical growth conditions.

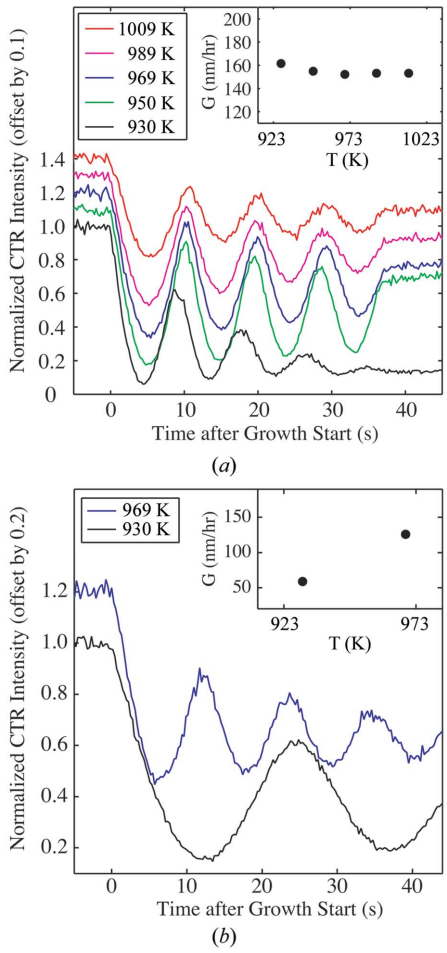

Figure 1
Evolution of 2 0 0.5 CTR intensity before, during and after growth of $PbTiO_3$ at various temperatures using fixed TEL and Ti precursor flows. (*a*) Growths with fixed TEL and TIP flows of 0.25 and 0.26 µmol min^{-1}, respectively. (*b*) Growths with fixed TEL and TTB flows of 0.25 and 0.95 µmol min^{-1}. Insets: growth rate as a function of temperature for fixed precursor flows.

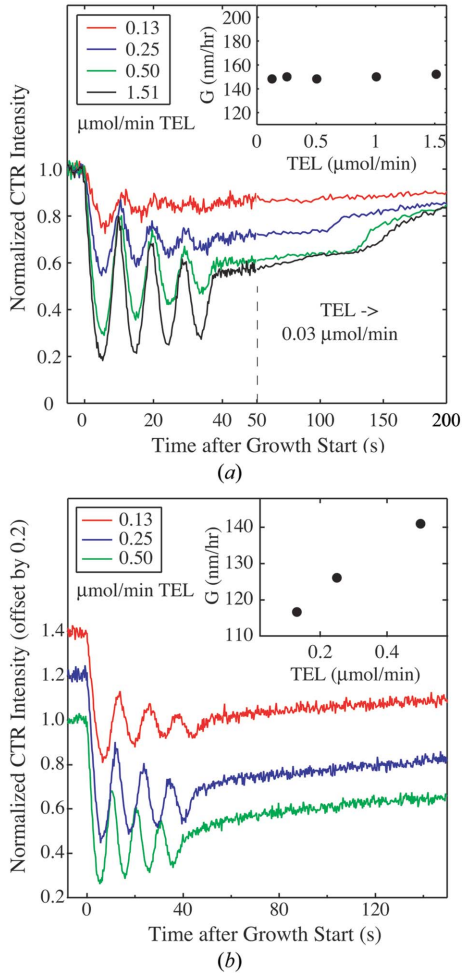

Figure 2
Evolution of the 2 0 0.5 CTR intensity before, during and after growth of ~16 Å $PbTiO_3$ at various TEL flow rates. (*a*) Growths with fixed TIP flow of 0.26 µmol min^{-1} at 1009 K. (*b*) Growths with fixed TTB flow of 0.95 µmol min^{-1} at 969 K. Insets: growth rate as a function of TEL flow.

In summary, for films grown with the TIP precursor, the rate of growth is limited only by Ti transport and is independent of temperature, TEL flow and P_{O_2}. The lack of a temperature dependence is in agreement with previous *ex situ* studies (Okada *et al.*, 1989; Dormans *et al.*, 1992), as is the linear dependence on TIP flow (Dormans *et al.*, 1992). We note that the Ti transport remains rate-limiting even for TIP/TEL ratios higher than unity. This suggests that the reactions converting TIP to adsorbed cations are less efficient than those for TEL. $PbTiO_3$ growth with the TTB precursor is more complex. The growth rate was found to increase with substrate temperature below 973 K, indicating that incomplete cracking of TTB may occur at lower temperatures.

3.2. Heteroepitaxial growth

When the film is thin enough, the X-rays can penetrate to the film/substrate interface, producing finite-thickness fringes along the CTR. As the thickness fringes form and sweep through a particular position, the CTR intensity there oscillates in time with a period proportional to the growth rate. Fig. 3 shows an example of such heteroepitaxial growth oscillations for the 20*L* CTR at L = 0.5. At this L position, each period of oscillation corresponds to the growth of two unit cells. The growth was performed at temperatures and deposition rates consistent with step-flow growth mode, thus producing only heteroepitaxial growth oscillations. These oscillations allowed us to monitor film thickness during growth to produce films of desired thickness for studies of the ferroelectric phase transition.

4. Equilibrium 180° stripe domains

For $PbTiO_3$ films coherently strained to the $SrTiO_3$ substrate, the ~1% compressive misfit strain causes polarization to occur preferentially along the surface normal. For $PbTiO_3$ films ~40 nm thick, the transition temperature, T_C, is elevated by more than 473 K above that of bulk $PbTiO_3$ owing to epitaxic strain, approaching the theoretically predicted value of 1025 K (Pertsev & Koukhar, 2000). However, T_C is observed to decrease strongly with film thickness.

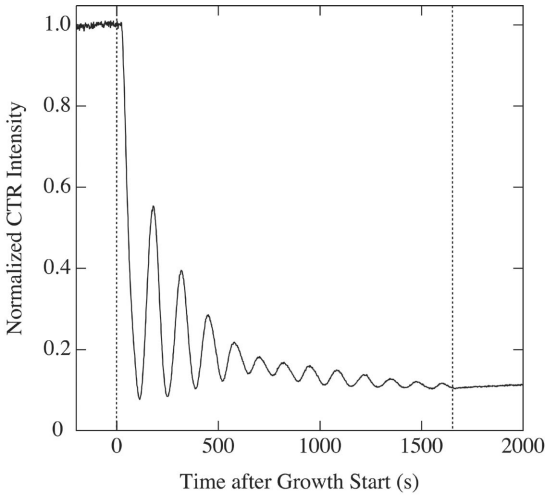

Figure 3
Heteroepitaxial growth oscillations of the 20L CTR at $L = 0.5$ during the growth of a 25 unit-cell-thick $PbTiO_3$ film on $SrTiO_3$ under step-flow growth conditions [$T = 969$ K, TTB:TEL = 1.6:1, growth rate = 0.016 unit cell s^{-1}, miscut = 0.23° (100 nm step spacing)] measured at $\alpha = \alpha_c$. Vertical dashed lines indicate the beginning and end of growth.

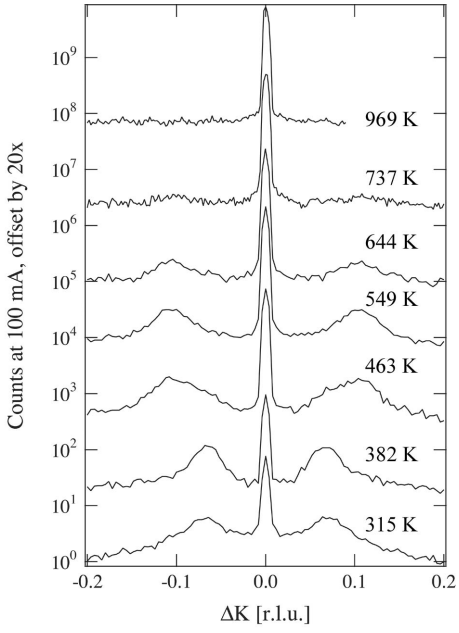

Figure 4
Sequence of scans through the $PbTiO_3$ 304 peak at various temperatures, showing the development of satellites during cooling for a 2.0 nm-thick film.

When a $PbTiO_3$ film is cooled below T_C, we observe the development of satellite peaks in the diffuse X-ray scattering adjacent to each $PbTiO_3$ Bragg peak. An example of this is displayed in Fig. 4, which shows data taken at various temperatures for a 2.0 nm film. The nature of this satellite scattering indicates that it comes from well ordered 180° stripe domains with alternating polarity. Satellites having the same spacing in H or K are observed at all $PbTiO_3$ Bragg peaks with the exception of those with $L = 0$, implying that the satellites originate from a spatial modulation rather than small rotations (as in the case of 90° domains), and that the atomic displacements causing the modulation are along the surface normal. The lack of even-order satellites is consistent with the expected 1:1 ratio of positive and negative domains, as required for electric field energy minimization. Satellites exhibit thickness fringes with the same periodicity as those on the CTR, showing that the modulation extends through the thickness of the film. At any given temperature, the positions and intensities of the satellites do not change with time and are reproducible, provided that the temperature is lowered monotonically from above T_C.

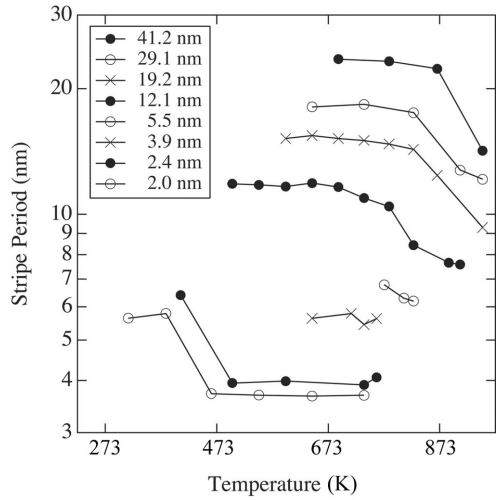

Figure 5
Stripe period as a function of temperature for $PbTiO_3$ films of various thicknesses.

The stripe period, Λ, may be determined from the in-plane scattering using

$$\Lambda = a/\left[(\Delta H)^2 + (\Delta K)^2\right]^{1/2},$$

where a is the reference lattice parameter for the reciprocal lattice units of H and K, in this case the room-temperature lattice parameter of $SrTiO_3$ (0.3905 nm). One can see in Fig. 4 that between 463 and 382 K the satellites shift in toward the Bragg peak. The decrease in ΔK corresponds to an increase in the stripe period. The stripe period is shown as a function of temperature in Fig. 5 for films of various thicknesses. At all thicknesses there is an abrupt change in period that we associate with a transition from a high-temperature stripe domain phase (F_α) to a low-temperature phase (F_β) with a larger stripe period. Higher-order satellites are often observed for the F_β phase, indicating that the 180° domain walls are less diffuse in F_β than F_α.

For both stripe phases the stripe period varies with the square root of film thickness. This parabolic thickness dependence is expected from the Landau–Ginzburg–Devonshire theory of ferroelectric 180° stripe domains (Kopal *et al.*, 1997; Mitsui & Furuichi, 1953) and results from the balance between the energy cost of domain walls and the energy gain in reducing the depolarizing field. We note that the stripe period for F_β agrees with theory within a factor of two on an absolute scale with no adjustable parameters (Streiffer *et al.*, 2002).

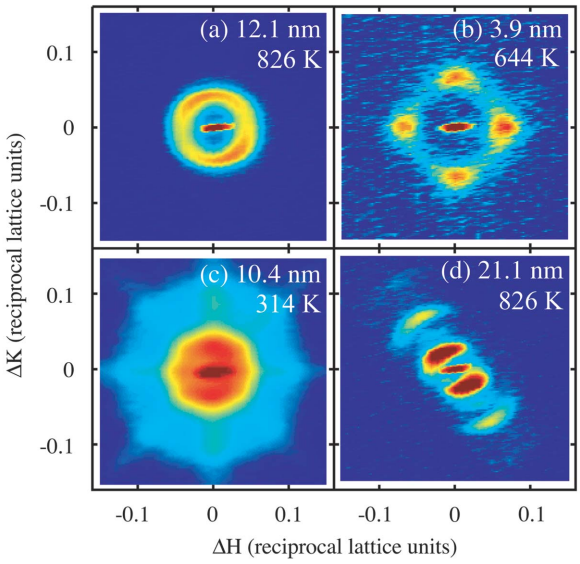

Figure 6
Typical in-plane distributions of diffuse X-ray intensity around the $PbTiO_3$ 304 peak for various film thicknesses and temperatures. Redder hues indicate higher intensity. The elongation of the central Bragg peak shows the asymmetric resolution function.

Typical in-plane arrangements of the satellite pattern are shown in Fig. 6. The satellites can either form rings (Fig. 6*a*), be aligned in crystallographic directions (Figs. 6*b*, 6*c*) or be aligned along a particular azimuth (Fig. 6*d*), depending on the temperature, film thickness and substrate miscut. These patterns are consistent with linear stripe domains oriented either randomly or in a specific direction within the illuminated area (1 mm^2). For thinner films, we often find that the crystallographically oriented stripes become randomly oriented near room temperature.

5. Conclusions

In summary, we have performed real-time and *in situ* X-ray scattering investigations of the growth and ferroelectric behaviour of $PbTiO_3$ thin films. The evolution of surface structure and morphology was measured by monitoring a CTR during growth. These experiments determined the influence of the substrate temperature and delivery rates of TIP, TTB and TEL on the growth mode and growth rate. It was observed that the different Ti precursors, TIP and TTB, behave very differently. For the TIP precursor the rate of growth is only limited by TIP transport, while for the TTB precursor the rate of growth depends on both substrate temperature and TEL flow as well as the TTB delivery rate.

We have also made the first observations of equilibrium 180° stripe domains in ferroelectric thin films. The stripes change structure upon cooling, transforming to a phase having a larger stripe period and sharper walls at lower temperature. Both stripe phases show a classical square-root thickness dependence. The ferroelectric transition temperatures of the thicker films studied here were significantly elevated above the unstrained bulk value owing to the compressive epitaxic strain; T_C, however, decreased with film thickness. A more detailed study of the effect of thickness on T_C is currently in progress.

We acknowledge assistance from L. Thompson, M. E. M. Aanerud and the BESSRC beamline staff. This work was supported by the US Department of Energy, BES-DMS under Contract No. W-31-109-ENG-38, and the State of Illinois under HECA.

References

Auciello, O., Scott, J. F. & Ramesh, R. (1998). *Phys. Today*, **51**, 22–27.
Bratkovsky, A. M. & Levanyuk, A. P. (2000*a*). *Phys. Rev. Lett.* **84**, 3177–3180.
Bratkovsky, A. M. & Levanyuk, A. P. (2000*b*). *Phys. Rev. Lett.* **85**, 4614–4617.
Bratkovsky, A. M. & Levanyuk, A. P. (2001). *Phys. Rev. B*, **63**, 132103.
Dormans, G. J. M., van Veldhoven, P. J. & de Keijser, M. (1992). *J. Cryst. Growth*, **123**, 537–544.
Kopal, A., Bahnik, T. & Fousek, J. (1997). *Ferroelectrics*, **202**, 267–274.
Lippmaa, M., Nakagawa, N., Kawasaki, M., Ohashi, S. & Koinuma, H. (2000). *Appl. Phys. Lett.* **76**, 2439–2441.
Mitsui, T. & Furuichi, J. (1953). *Phys. Rev.* **90**, 193–202.
Munkholm, A., Streiffer, S. K., Murty, M. V. R., Eastman, J. A., Thompson, C., Auciello, O., Thompson, L., Moore, J. F. & Stephenson, G. B. (2002). *Phys. Rev. Lett.* **88**, 016101.
Muralt, P. (2000). *J. Micromech. Microeng.* **10**, 136–146.
Murty, M. V. R., Streiffer, S. K., Stephenson, G. B., Eastman, J. A., Bai, G.-R., Munkholm, A., Auciello, O. & Thompson, C. (2002). *Appl. Phys. Lett.* **80**, 1809–1811.
Okada, M., Takai, S., Amemiya, M. & Tominaga, K. (1989). *Jpn. J. Appl. Phys.* **28**, 1030–1034.
Pertsev, N. A. & Koukhar, V. G. (2000). *Phys. Rev. Lett.* **84**, 3722–3725.
Pertsev, N. A., Zembilgotov, A. G. & Tagantsev, A. G. (1998). *Phys. Rev. Lett.* **80**, 1988–1991.
Polla, D. L. & Francis, L. F. (1996). *MRS Bull.* **21**, 59–65.
Rijnders, G. J. H. M., Koster, G., Blank, D. H. A. & Rogalla, H. (1997). *Appl. Phys. Lett.* **70**, 1888–1890.
Speck, J. S. & Pompe, W. (1994). *J. Appl. Phys.* **76**, 466–476.
Stephenson, G. B., Eastman, J. A., Auciello, O., Munkholm, A., Thompson, C., Fuoss, P. H., Fini, P., Den Baars, S. P. & Speck, J. S. (1999). *MRS Bull.* **24**(1), 21–25.
Streiffer, S. K., Eastman, J. A., Fong, D. D., Thompson, C., Munkholm, A., Murty, M. V. R., Auciello, O., Bai, G.-R. & Stephenson, G. B. (2002). *Phys. Rev. Lett.* **89**, 067601.
Terashima, T., Bando, Y., Iijima, K., Yamamoto, K., Hirata, K., Hayashi, K., Kamigaki, K. & Terauchi, H. (1990). *Phys. Rev. Lett.* **65**, 2684–2687.
Wang, Y. G., Zhong, W. L. & Zhang, P. L. (1995). *Phys. Rev. B*, **51**, 5311–5314.